sustainability

MDPI

Article

Experimental Investigation of Particle Size Alteration and the Selective Crushing Phenomenon of Gangue during the Jaw Crushing Process

Lei Zhu [1], Wenzhe Gu [1,2,*], Tianqi Song [1] and Fengqi Qiu [1]

[1] China Coal Energy Research Institute, Xi'an 710054, China
[2] School of Energy and Mining Engineering, China University of Mining and Technology, Beijing 100083, China
* Correspondence: guwenzhe7@163.com; Tel.: +86-180-9253-5618

Abstract: This study examines the particle size and distribution of the main chemical components of gangue during the crushing process. Coal mine gangue was chosen as the research object, and its particle size and chemical components at various crusher discharge settings were examined through screening, grinding, chemical composition testing, and other methods. The findings demonstrate that the characteristic particle size in the gangue particle size distribution model has a logarithmic upward trend as the width of the discharge port increases. In contrast, the uniformity index has shown an exponential downward trend. The analysis of the distribution rate and enrichment ratio of the main chemical components of the gangue at different widths of the discharge port shows that the gangue exhibits obvious selective crushing during the crushing process. The distribution rate of each component is affected by the size of the screen aperture to various extents. As the discharge port width increases, the elements of CaO and MgO are enriched in the coarse-grained products, while those containing Fe_2O_3 are enriched from fine-grained to coarse-grained. Gangue particles containing Al_2O_3, SiO_2, and C are enriched in the fine-grained product. In addition, by analyzing the alterations in the main chemical components of gangue at different particle size intervals, it was found that the amount of each component first rises and then falls, and the trend of enrichment ratio to particle size follows an exponential pattern. The research results have significance for guiding the selection of resource utilization methods of gangue with different particle sizes after crushing.

Keywords: gangue; jaw crushing; particle size distribution; elemental analysis; selective crushing

check for updates

Citation: Zhu, L.; Gu, W.; Song, T.; Qiu, F. Experimental Investigation of Particle Size Alteration and the Selective Crushing Phenomenon of Gangue during the Jaw Crushing Process. *Sustainability* **2022**, *14*, 12395. https://doi.org/10.3390/su141912395

Academic Editors: Peng Li, Yanxia Guo, Baolin Xing and Quanzhi Tian

Received: 14 August 2022
Accepted: 14 September 2022
Published: 29 September 2022

1. Introduction

As the current primary fossil energy and the main driving force for economic and social development, the large-scale mining and utilization of coal resources, accompanied by large amounts of coal gangue, is continuous and produces an annual output of 800 million to 1 billion t/a. Except for the comprehensive utilization of small amounts, most of the coal gangue is accumulated and stored in nearby areas, which greatly harms and seriously impacts the ecological environment [1–3]. Therefore, to effectively solve the problems caused by bulk solid waste such as gangue, scholars at home and abroad have conducted research on the full development and utilization of coal gangue for decades and have achieved many results [4–7]. Dang et al. [8] developed high-strength and lightweight glass ceramics by optimizing parameters such as the amount of coal gangue, mineralizer, and clay. At the same time, the mechanical properties of the materials were improved by optimizing the process parameters. Finally, an excellent method for sintering glass ceramics was developed, characterized by high strength, light weight, and low water absorption. Xu [9] used crushed gangue, limestone, and gypsum as the main materials and fluorite and barite as the secondary materials and prepared an alite-sulfoaluminate cement at 1330 °C. The results showed that the compressive strength of the cement after 7 days was 48.9 MPa. Wang [10] prepared a new biochar composite material using crushed coal gangue as a

raw material in a one-step pyrolysis method. Numerous studies have shown that coal gangue-modified biochar composites can be used not only for phosphorus removal from wastewater but also as slow-release fertilizers, providing a new method for the recovery and resource utilization of phosphorus from solid wastes. In addition, many studies have been conducted on the use of coal gangue in power generation, filling, building materials, light-weight aggregates, and the extraction of chemical products [11–14].

However, it is clear from the aforementioned studies that in order to use gangue as a resource, it must first be crushed, and various utilization techniques have strict requirements for the gangue's chemical composition and particle size. Whether the chemical components of gangue will migrate along with the grain size after dynamic crushing and what migration rules are among the components are the preconditions for judging which resource utilization method the broken gangue will be used in. This is not covered in existing research. However, the existing research on gangue particle size and composition analysis mainly focuses on gangue's particle size under static compression or dynamic impact loading [15,16]. Wu [15] studied the mechanical behavior of gangue filling materials in depth. Through the physical compression test and particle flow numerical simulation of red sandstone gangue with different particle sizes, the bearing characteristics of gangue compaction were comprehensively compared and analyzed from macro and micro perspectives. The deformation failure laws were also discussed. Song et al. [16] studied the compaction and re-compaction characteristics of different grades of coal gangue and conducted a compaction fractal test on coal gangue with different talbol power exponents. The test results analyzed the compaction deformation parameters of coal gangue, such as displacement and stress-strain. Li [17] used an impact crusher to conduct impact crushing tests on gangue at different impact speeds. The effects of the impact velocity and coal gangue hardness on the coal gangue particle size distribution function were obtained through the data fitting of the experimental results. Yang [18] conducted impact experiments on gangue based on uniaxial compression experiments. According to the Rosin–Rammler distribution law, the particle size distribution of coal and gangue at different impact speeds was studied by collecting and sieving the broken coal gangue particles. The relationship between the separation index and impact velocity was discussed. However, most of the studies on element separation in gangue are focused on leaching tests. For example, Zhang H et al. [19,20] conducted leaching tests on coal gangue in the laboratory to study the migration mechanism and laws of harmful metals in coal gangue. The concentration of each element in the leaching water was changed, and the factors affecting the dissolution and release rate of each element in the gangue were obtained. Li [21] simulated the leaching and precipitation characteristics of heavy metals in low-sulfur coal gangue under different environmental conditions through indoor dynamic leaching experiments, which provided a theoretical basis for environmental restoration in mining areas. The results showed that the higher the content of heavy metals in low-sulfur coal gangue, the greater the leaching of heavy metals; the acidic conditions promote the release of heavy metals in low-sulfur coal gangue. Previous studies have shown that although there are many possible applications for gangue, the chemical composition of gangue itself determines the type of gangue resource utilization [22–26]. Therefore, the scientific utilization of gangue with different crushed particle sizes needs to be determined according to the composition of the crushed gangue.

Based on the above-discussed literature, it can be concluded that there are few existing studies on the analysis of particle size and chemical composition of gangue after jaw crushing. In fact, due to differences in the natural friability of minerals, the jaw crushing process inevitably increases the particle size differences between minerals, resulting in fluctuations in the composition of the gangue at the different particle sizes. To unveil the distribution of gangue particle size after mechanical crushing and to examine the distribution of the main chemical components of gangue, it is necessary to study the crushed particle size of gangue using crushing equipment. The findings of this research will provide significant direction for the crushing process and the utilization of gangue resources.

2. Materials and Methods

2.1. Raw Material Preparation

The gangue used in this research was taken from the Mahuangliang Mine in the southeast of the Yushen Mining Area (Yulin City, Shaanxi Province), a mine under construction. The minefield has a simple geological structure. The current main coal seam is a #3 coal seam, with a buried depth of 180–210 m and a coal seam thickness of 9.06 m. The gangue produced during mining mainly comes from coal bed gangue and roof gangue (Figure 1). It can be seen from the stratigraphic map that the gangue lithology is mainly mudstone, carbonaceous mudstone, silty mudstone, and argillaceous siltstone.

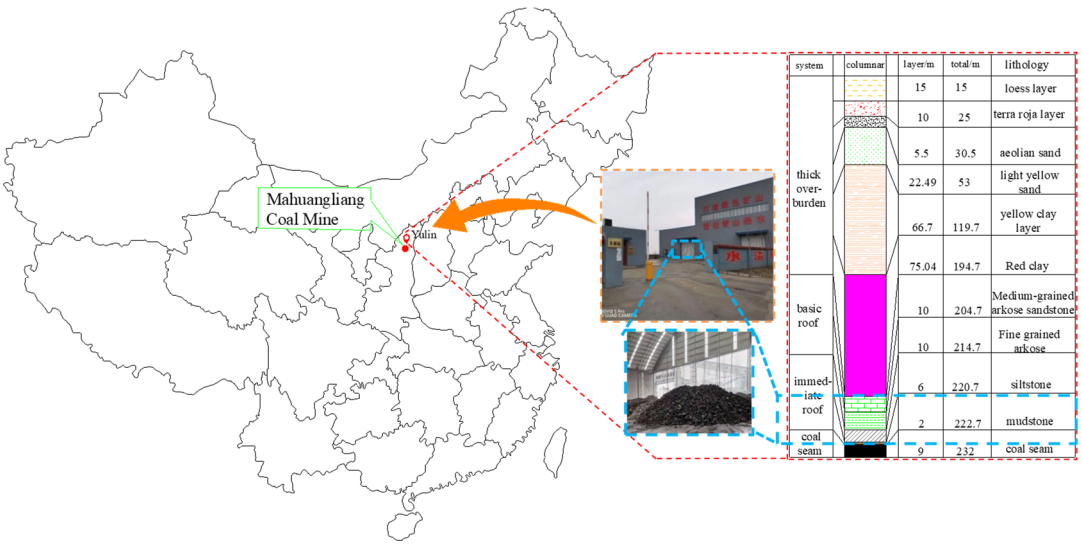

Figure 1. Geological conditions and gangue sampling sites of Mahuangliang mine.

2.2. Test Equipment

The gangue crushing equipment used in the experiment is a jaw crusher which is also traditional ore-crushing equipment commonly used in mines. Due to its simple structure and reliable operation, it is one of the most widely used mechanical equipment for gangue crushing [22,27]. The model of the indoor jaw crusher is PEF60 × 100, and the maximum feeding particle size is 100 mm. The width of the discharge port can be adjusted from 6 to 10 mm.

The phase and composition of the crushed gangue were analyzed by the XRF-1800 scanning X-ray fluorescence spectrometer and the D/max2550 automatic X-ray diffractometer. The XRF instrument comprises an excitation source (X-ray tube) and a detection system. The instrument has ultra-high-speed analysis capabilities and an effective element measurement range from O^8 to U^{92}. The D/max2550 automatic X-ray diffractometer uses a voltage of 40 kV, a scan rate of 8 deg/min, and a scan range of 2–80° (2-theta).

However, the gangue contains carbon, which is an important manifestation of its difference from other rocks and a parameter that XRD and XRF cannot directly test. Therefore, the calculation of carbon content was carried out according to the standard GBT 35986-2018 "Determination of Loss on Ignition of Coal Gangue", and the loss on ignition was tested and then indirectly obtained using the loss on ignition. The specific method is as follows:

Assuming that the other conditions remain unchanged, the ignition loss is caused by the thermal decomposition of $CaCO_3$ and $MgCO_3$ to release CO_2 and the combustion of C to generate CO_2. Assuming that the loss on ignition is a%, the percentages of CaO and MgO are b% and c%, respectively.

$$\begin{cases} CaCO_3 \rightarrow CaO + CO_2 \\ \quad\quad\quad 56 \quad\quad 44 \\ \quad\quad\quad b \quad\quad 44b/56 \end{cases} \begin{cases} MgCO_3 \rightarrow MgO + CO_2 \\ \quad\quad\quad 40 \quad\quad 44 \\ \quad\quad\quad b \quad\quad 44b/40 \end{cases} \begin{cases} C + O_2 \rightarrow CO_2 \\ 12 \quad\quad\quad 44 \\ x \quad a - (44b/56) - (44c/40) \end{cases}$$

Then, the percentage of carbon is calculated using: $\frac{12\times(a-\frac{44b}{56}-\frac{44c}{40})}{44}$.

2.3. Scheme Design

The test involved in this research is divided into two parts: gangue-crushing particle size statistics and chemical composition analysis. The specific test flow chart is shown in Figure 2.

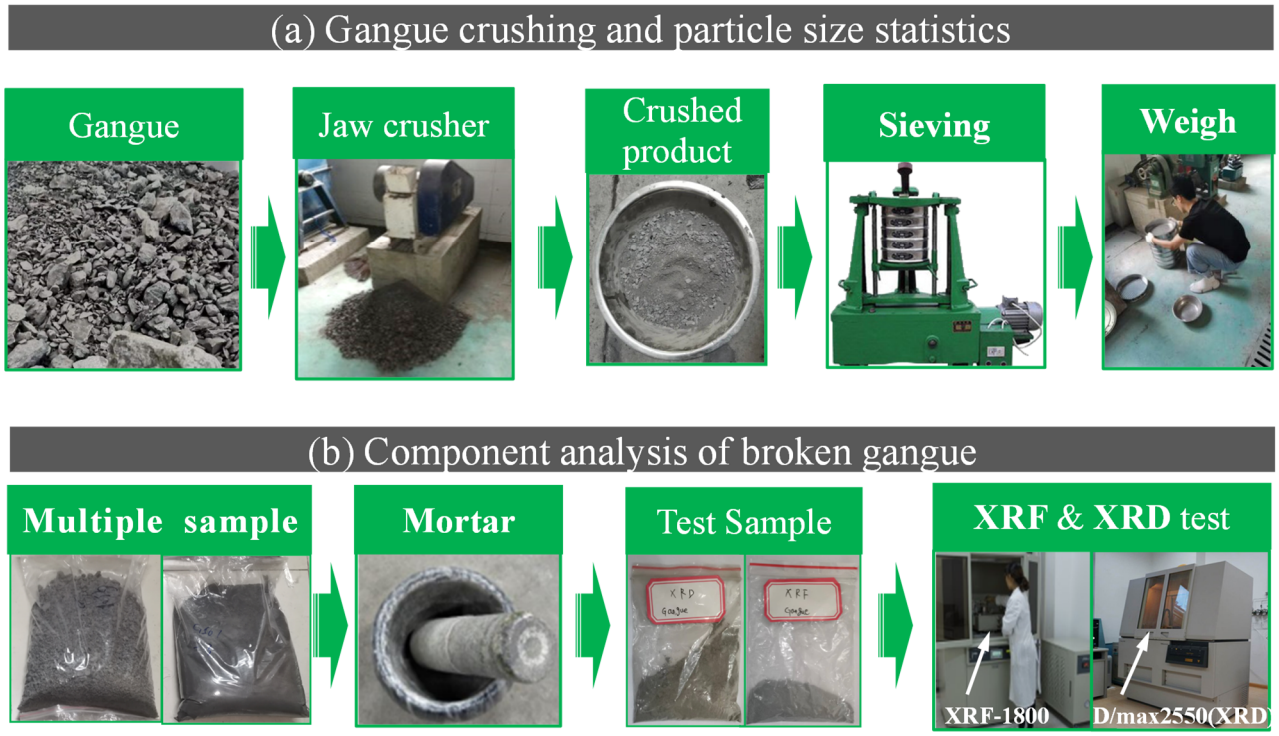

Figure 2. Grain size statistics and composition analysis of gangue.

Through crushing tests on three groups of originally graded gangue with various discharge port widths, the alterations in the particle size of gangue at different discharge port widths were investigated. Using statistical research on crushing particle size and adjusting the width of the discharge port of the jaw crusher, the gangue was crushed once, and then, the crushed gangue was screened and weighed; the particle size distribution of the gangue at different discharge port widths we calculated (Figure 2a). In order to study the selective crushing phenomenon in the process of gangue crushing, as shown in Figure 2b, the gangue in a range of particle sizes was grounded after crushing, and its chemical composition was analyzed by means of XRD and XRF.

3. Results and Discussion

3.1. Particle Size Distribution of Jaw-Crushed Gangue

In order to describe the functional relationship between gangue particle size and proportion, the particle size distribution of jaw-crushed gangue was explored. Firstly, standard sieves were utilized to classify the particle size of the gangue, and then, the mass proportion of the gangue in each particle size range after sieving was counted. The Rosin–Rammler formula (abbreviated as "R–R") is used to statistically analyze the particle size distribution of the gangue [28–31]. The formula is expressed as follows (Equation (1)):

$$R(D_p) = 1 - \exp\left[-\left(\frac{D_p}{D_e}\right)^n\right] \quad (1)$$

In Equation (1), $R(D_p)$ represents the cumulative (%) characteristic particle size of the sieve residue and n represents the uniformity index, which characterizes the breadth and narrowness of the particle size distribution range. The original particle size distribution curve (Figure 3) and gangue's function expression are obtained using Matlab fitting and statistics. For this, the gangue collected at the mine site was used as an example.

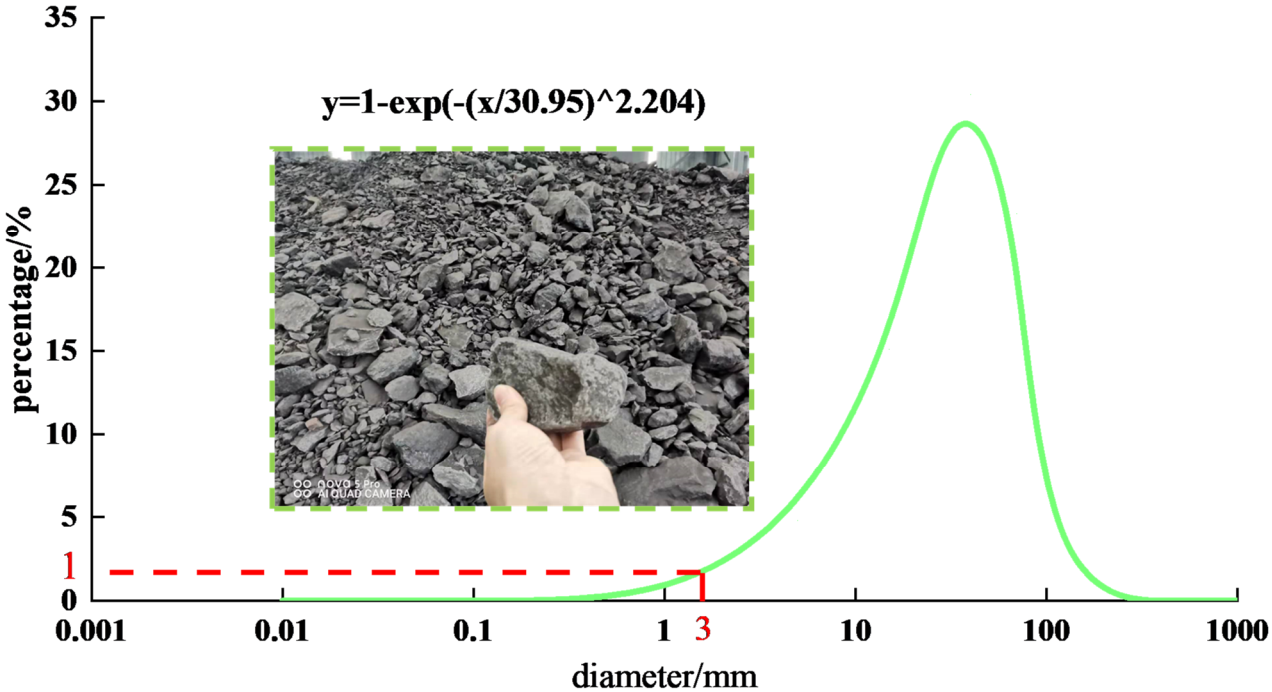

Figure 3. Grain size distribution curve of original gangue.

Figure 4 shows the R–R relationship curve of the gangue particle size distribution at different discharge port widths in double logarithmic coordinates. It can be seen from Figure 4 that the regression curve of the scatter plot at any width of the discharge port is a straight line, and the smallest square of the regression coefficient is $R^2 = 0.978$, which is in good agreement with the R–R distribution function. It is also evident from Figure 4 that the uniformity index n decreases with the increase of the discharge port width. This is because in the double logarithmic lnd-ln{-ln [1-R(*dp*)]} coordinate system, the slope of the regression line is constantly decreasing slightly from 1.146 (when the width of the discharge port is 6mm) to 1.083 (when the width is 10 mm).

$$\begin{cases} y = 1.146x - 1.996 \\ y = 1.1x - 2.61 \\ y = 1.083x - 2.81 \end{cases} \rightleftarrows \begin{cases} R(D_p) = 1 - \exp(-(D_p/5.71))^{1.146} \\ R(D_p) = 1 - \exp(-(D_p/10.72))^{1.1} \\ R(D_p) = 1 - \exp(-(D_p/13.35))^{1.083} \end{cases} \quad (2)$$

The particle size distribution of the gangue is depicted in Figure 5, where the width of the discharge port is 6–10 mm into the particular Formula (2) of the particle size distribution. This was obtained from the linear regression line equation (Figure 5). It can be seen from Figure 5 that the gangue was broken under the influence of the discharge port widths. It was found that, overall, the particle size distribution trend of the gangue under the width of each discharge port is consistent and follows a normal distribution as the width of the discharge port increases. The characteristic particle size of gangue rises exponentially with the increase of the discharge port width, from 5.71 mm at a discharge port width of 6 mm to 13.35 mm at a discharge port width of 10 mm.

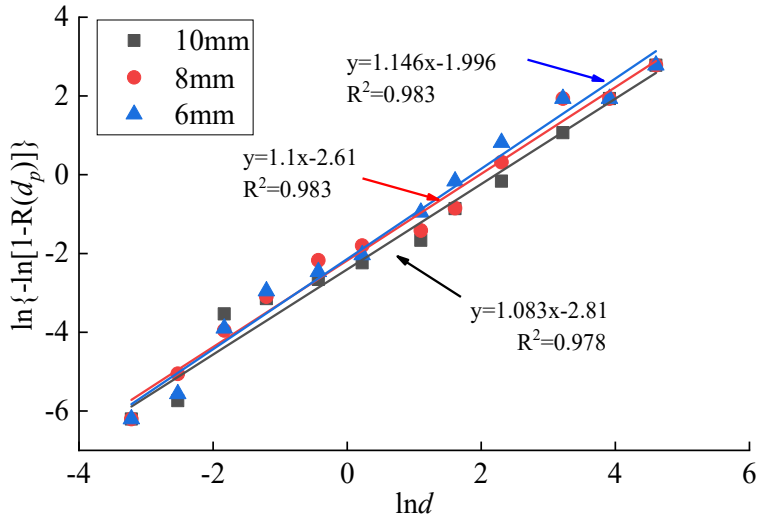

Figure 4. R–R relation curves at different ore port widths in the double logarithmic coordinates system.

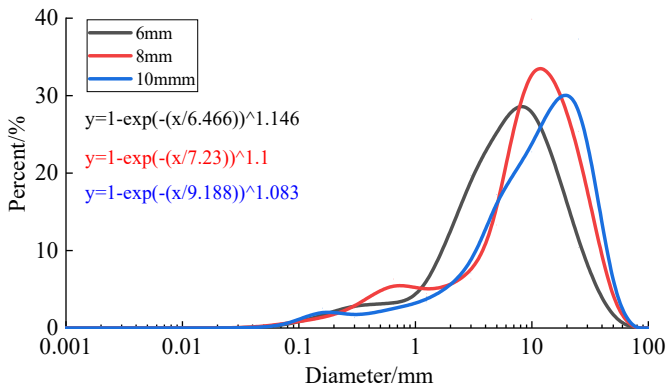

Figure 5. The particle size distribution of gangue at different discharge ports.

Figure 6 shows the variations in the characteristic particle size and uniformity index at different discharge port widths. It can be seen from Figure 6 that as the width of the discharge port increases, the particle size D_e of the characteristic value increases logarithmically, and the obtained expression is

$$D_e = 7.39 * ln(x - 3.82) \tag{3}$$

In contrast, the uniformity index n decreases exponentially, and the expression is

$$n = 1.399 * x^{-0.1129} \tag{4}$$

This is because as the width of the discharge port increases, each particle size distribution of gangue within the particle size range becomes wider, and the uniformity decreases. From the above analysis and data fitting, the particle size distribution model of the jaw crusher with different discharge port widths is expressed as

$$R(D_p) = 1 - \exp\left[-\left(\frac{D_p}{7.39 * \ln(\mathrm{x} - 3\ .82)}\right)^{1.399 * x(-0.1129)}\right] \tag{5}$$

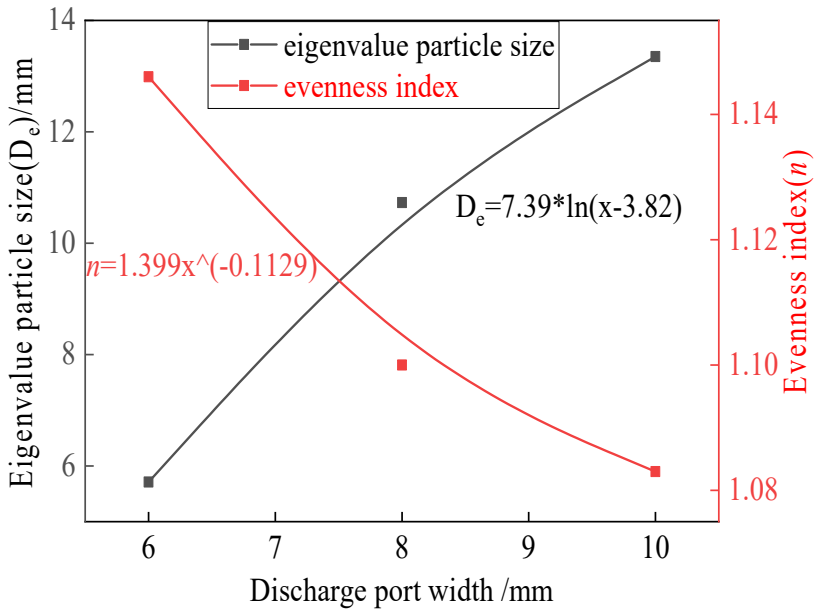

Figure 6. Changes in particle size and uniformity index of gangue characteristic value after jaw crushing.

3.2. Research on the Phenomenon of Selective Crushing of Gangue

Previous studies have shown that although there are many possible applications for gangue, the chemical composition of the gangue itself determines the utilization of the gangue resource [28–31]. Therefore, the scientific utilization of gangue with different crushed particle sizes needs to be determined according to its composition. To this end, the author conducted grinding and elemental analyses on products with different particle sizes after crushing to explore the distribution of elements at different particle size ranges and reveal the selective crushing phenomenon of gangue.

The scan results were analyzed by Jade to obtain the gangue phase composition. Figure 7 shows the phase composition of the gangue (XRD test results) and the proportion of main components (XRF test results). The results illustrate that the phase composition of the selected gangue mainly includes Quartz (SiO_2), Gypsum ($CaSO_4$), Kaolinite ($Al_2O_3{\cdot}2SiO_2{\cdot}2H_2O$), Mica ($(KAl_2(AlSi_3O_{10})(OH)_2)$), Ankerite ($CaMg(CO_3)_2$), etc. The main chemical components, and their proportions, are SiO_2 (59.65%), Al_2O_3 (22.7%), Fe_2O_3 (5.703%), CaO (3.217%), MgO (2.02%), C (0.37%), etc.

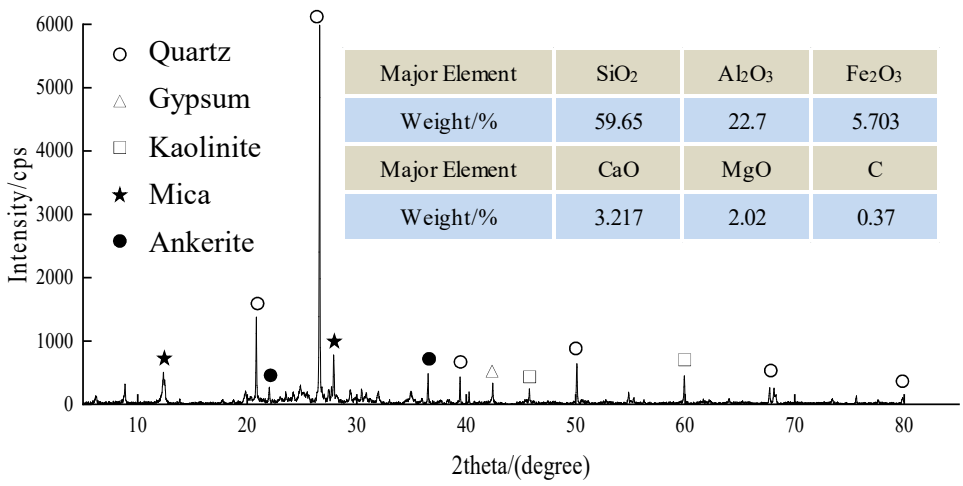

Major Element	SiO_2	Al_2O_3	Fe_2O_3
Weight/%	59.65	22.7	5.703
Major Element	CaO	MgO	C
Weight/%	3.217	2.02	0.37

Figure 7. Phase composition and proportion of main components of gangue.

Two indicators, the distribution rate (ε) and the enrichment ratio (θ), which are similar to the beneficiation evaluation indicators, were introduced to quantify the changes in chemical composition after crushing [32–34]. The distribution rate (ε) refers to the percentage of a certain component's content in the product of a certain grade to the component's content in the original ore sample expressed by Equation (6). The distribution ratio (ε) can investigate the distribution of each component in the raw ore sample in the two grades of products. The enrichment ratio (θ) is similar to the ratio of concentrate grade to raw ore grade in the beneficiation evaluation index, expressed in Equation (7), which measures the enrichment ratio of a certain mineral in a certain particle size product.

$$\varepsilon = \gamma \cdot \frac{\beta}{\alpha} \tag{6}$$

$$\theta = \frac{\beta}{\alpha} \tag{7}$$

In Equations (6) and (7), α represents the percentage content (%) of a mineral in the original ore; β represents the percentage content (%) of a mineral in the two grades of products; and γ represents the yield (%). Furthermore, γ represents the mass fraction of each particle size after crushing, which is obtained by testing the ratio between the mass of each part of gangue and the total mass (Figure 2a), and parameters such as α and β, which represent the elemental composition, are obtained by XRD and XRF tests (Figure 2b).

3.2.1. Element Enrichment at Different Discharge Ports Widths

The classification of granular objects in powder mechanics is introduced to study the selective crushing phenomenon of gangue at different discharge port widths [35]. For the test, a 3 mm particle size limit is used to categorize the crushed gangue into fine and coarse grain gangue. Particulate material (−3 mm) and crushed solid material (+3 mm) are referred to as fine particle size and coarse particle size, respectively. It can be seen from Figure 3 that the −3 mm gangue particles in the original gangue account for about 1.0%. Therefore, the −3 mm gangue obtained after crushing can be regarded as a product of jaw crushing.

Figure 8 elucidates the particle size distribution of crushed gangue and the yields of +3 mm and −3 mm particles at different discharge port widths. It can be seen from Figure 8 that the particle size distribution at each discharge port width conforms to the particle size distribution model in Section 3.1. As the width of the discharge port increases, the yield of the +3 mm particles gradually increases, and the yield of the −3 mm particles gradually decreases.

Table 1 shows the proportion of the chemical components in the two grades of products under different ore discharge conditions. Table 1 shows the percentage content of each gangue component in the two grades of products after crushing compared to the original ore, and significant alterations have occurred. The mineral distribution depends on the amount that goes into that fraction. In order to further investigate the separation and enrichment of the elements, the separation effect of the main components in the gangue was analyzed, and the distribution rate (ε) and enrichment ratio (θ) of each component were calculated. The obtained results are shown in Figures 9 and 10.

Figure 9 shows the change in the element distribution rate (ε) in the gangue of various particle sizes. According to the changing trend of the distribution rate (ε) of each element displayed in Figure 9a, they can roughly be divided into two categories. The distribution rate (ε) of type I (SiO_2, Al_2O_3, Fe_2O_3, CaO, MgO) always increases with the width of the discharge port, indicating that the larger the width of the discharge port, the greater the distribution rate (ε) of these components in the coarse fraction. The distribution rate (ε) of type II (C) in coarse-grained products decreases with the increase in discharge port width because the substances containing $CaCO_3$ and $MgCO_3$ (magnesium carbonate) are also distributed into the coarse-grained products. At the same time, C in gangue tends to be distributed in −3 mm particle size products. Figure 9b shows that the distribution ratio (θ)

of each element in the fine-grained product changes with the width of the discharge port. Except for element C, all other components decrease with the increasing width, indicating that the elements containing C gradually enter the fine-grained product, expanding their distribution rate (ε) in the fine-grained product. Figure 9a,b show a significant variation between the distribution ratios of the aforementioned components in the two granular products. From the $\Delta\varepsilon_{max}$ (referring to the difference between the ε-max value and the ε-min value at different widths of discharge ports) for each element, it is clear that the influence of the width of the discharge port on each component is in the following order: Fe_2O_3 > SiO_2 > Al_2O_3 > C > MgO > CaO. The corresponding percentages of each mineral follow this order: 36.00% > 19.83% > 15.54% > 14.43% > 9.51% > 8.38%.

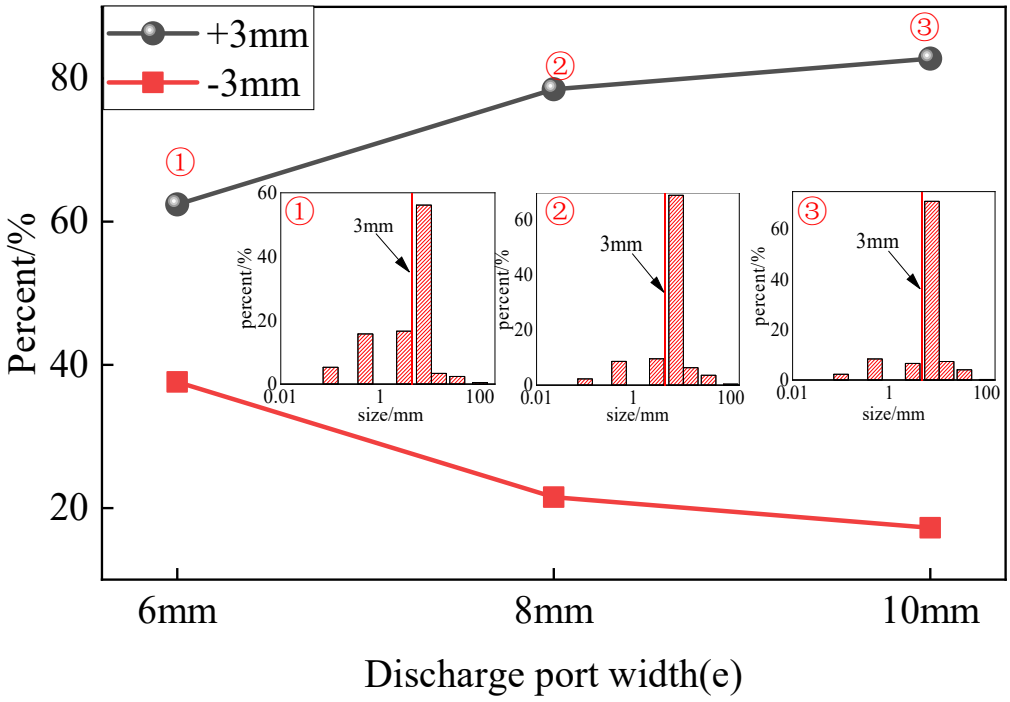

Figure 8. The particle size distribution of gangue crushing and the yield of +3 mm and −3 mm particles at different discharge port widths.

Table 1. Proportion of each component at different widths of discharge ports.

Width	SiO_2 (%)		Al_2O_3 (%)		Fe_2O_3 (%)		CaO (%)		MgO (%)		C (%)	
	+3 mm	−3 mm	+3 mm	−3 mm	+3 mm	−3 mm	+3 mm	−3 mm	+3 mm	−3 mm	+3 mm	−3 mm
6 mm	57.54	62.67	20.49	24.12	5.77	6.03	4.61	0.75	3.05	0.58	0.12	1.13
8 mm	56.15	65.32	20.07	25.66	5.90	4.12	4.76	0.48	3.16	0.29	0.05	1.54
10 mm	56.02	66.32	22.01	26.09	5.93	0.77	4.91	0.13	3.22	0.12	0.01	1.74

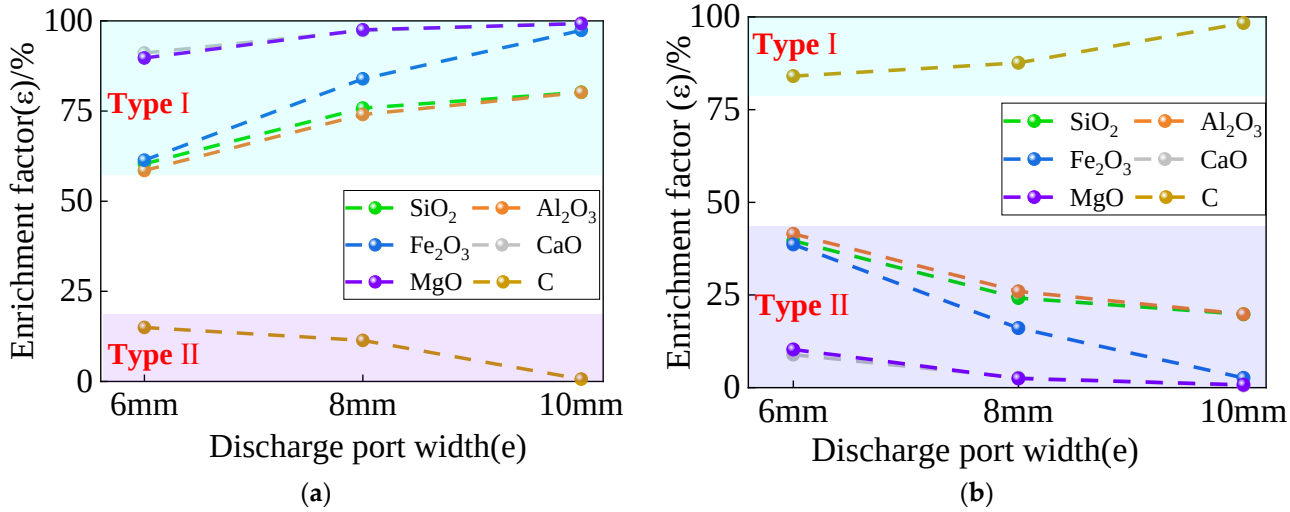

Figure 9. Distribution ratio of elements in gangue with different particle sizes. (**a**) +3 mm. (**b**) −3 mm.

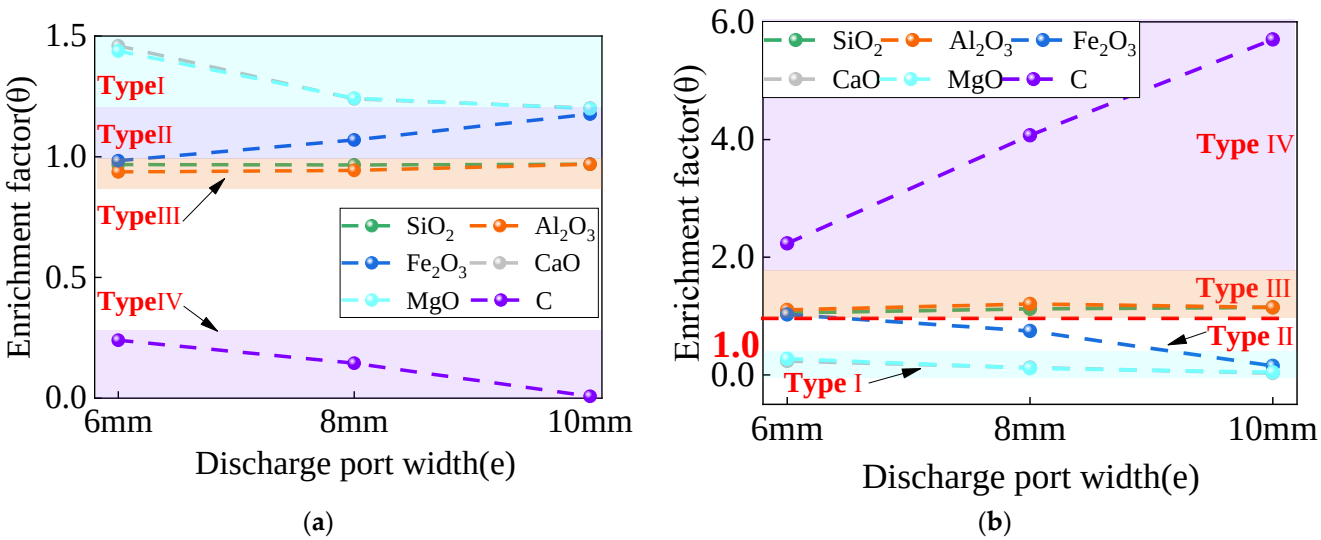

Figure 10. Element enrichment in gangue with different particle sizes. (**a**) +3 mm. (**b**) −3 mm.

Figure 10 shows the enrichment of elements in the two-part particle size gangue. According to the variation in the enrichment ratio (θ) of each component with the width of the discharge port, the components in Figure 10a can be divided into four categories. The enrichment ratio (θ) of type I (including CaO and MgO) was always greater than 1.0 in the coarse-grained products. The enrichment ratio (θ) increased gradually as the discharge port width decreased. This shows that the proportion of coarse-grained products is always larger than that of the raw ore. According to Figure 7, this is because the components containing CaO and MgO, such as gypsum and dolomite, are difficult to break [36], resulting in the enrichment of CaO, MgO, and other components in large particles. The enrichment ratio (θ) of type II (including Fe_2O_3) fluctuated around 1.0 and gradually increased with the increase of the width of the discharge port, indicating that with the increasing discharge port, Fe_2O_3 gradually enriches from fine to coarse particles. The enrichment ratio (θ) of type III (including Al_2O_3 and SiO_2) increased slowly with the increase of the width of the discharge port, and the range was concentrated between 0.95 and 1.0; the change in enrichment ratio (θ) was not particularly significant. The reason may be that some of the SiO_2 were stored in clay minerals with little hardness [37], and some were deposited in silicate minerals with significant hardness, such as calcium silicate. As a result, the

enrichment ratio of type III in the coarse and fine particle size is less affected by the discharge port, and the two particle-size products are seriously mixed. The enrichment ratio (θ) of type IV (including C) was always less than 1.0 and decreased with the increase of the width of the discharge port, indicating that C is mainly enriched in the fine-grained products after crushing compared with the original ore. According to the analysis in Figure 7, it can be seen that the phase composition containing Al_2O_3, SiO_2, and C mainly consisted of kaolinite, mica, carbon, and other substances. These substances are relatively easier to break due to their low strength [38–40]; thus, they were broken and enriched in the fine-grained products. Similarly, Figure 10b shows the enrichment of elements in the fine-grained gangue, and the changing trend of the enrichment ratio (θ) of each component in the fine-grained gangue is opposite to that in the coarse-grained gangue. In conclusion, in the jaw crushing process, the gangue particles containing CaO and MgO are enriched in the coarse-grained products as the width of the discharge port increases. The particles containing Fe_2O_3 in the gangue gradually concentrated from fine-grained to coarse-grained, and the gangue particles containing Al_2O_3, SiO_2, and C were more easily broken and enriched in the fine-grained products.

3.2.2. Elemental Enrichment at Different Particle Sizes

The gangue samples obtained when the width of the ore port was 6mm were chosen for component analysis in five particle size ranges of <1 mm, 1–2.5 mm, 2.5–5 mm, 5–10 mm, and >10 mm, respectively, to investigate the elemental distribution in various particle size ranges. Table 2 summarizes the yields and element ratio in different particle size regions.

Table 2. Element distribution in different particle size ranges.

Size/mm	Yield/%	Element Ratio/%					
		SiO_2	Al_2O_3	Fe_2O_3	CaO	MgO	C
<1	12.7	67.32	26.09	0.27	0.13	0.12	1.59
1–2.5	13.26	64.31	25.48	1.67	0.53	0.40	1.57
2.5–5	31.67	60.10	22.75	3.82	2.94	2.58	0.72
5–10	27.42	57.54	20.49	5.77	4.61	3.05	0.39
>10	14.95	55.10	18.41	7.05	5.53	4.54	0.02

Compared with the original ore, the percentages of CaO, SiO_2, $A1_2O_3$, and Fe_2O_3 in the gangue after crushing changed greatly in each grade, as depicted in Figure 7 and Table 2. Figure 11 shows the distribution rate (ε) of each component at different particle size ranges. According to a thorough investigation of the variation law of each component of the gangue with crushed particle size, the distribution rate (ε) of each element exhibits a law of first increase and then decrease. This is because, in the jaw-crushing process, the gangue yield distribution of each particle size was normally distributed in the region; thus, the distribution rate (ε) of each component also increased first and then decreased when affected by the yield. Correspondingly, by comparing the $\Delta\varepsilon_{max}$ of each component in Figure 11, it can be seen that the effect of particle size on each component is C > MgO > CaO > Fe_2O_3 > Al_2O_3 > SiO_2. Additionally, from the analysis of the proportion of the main components of gangue in Table 2, it can be seen that the particles containing C have lower hardness and are relatively easier to break. They could easily be distributed as small particles after crushing and rarely appeared in large particles. The particles containing MgO and Cao were mainly gypsum and dolomite, which were not fully broken due to their high hardness; thus, they almost did not exist in small particle sizes. Therefore, particle size has a great influence on C, MgO, and CaO. In comparison, Al_2O_3, Fe_2O_3, and SiO_2 mainly exist in mica, kaolinite, and quartz, which include clay minerals with lower hardness and silicate minerals with higher hardness. Therefore, the separation effect was not significant due to the influence of particle size.

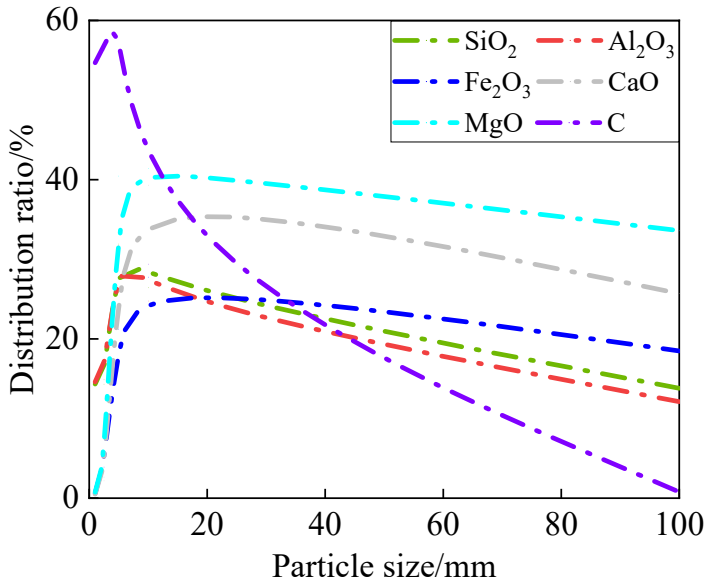

Figure 11. Distribution of elements in gangue at different particle sizes.

Figure 12 shows the enrichment of each component in gangue at different particle sizes. It can be seen from Figure 12 that the trend of each component changes with particle size in the form of "$y = a + b * c^x$". Among them, the enrichment ratios of SiO_2, Al_2O_3, and C decreased with the increase of particle size (b > 0), and MgO, CaO, and Fe_2O_3 decreased with the increase of particle size (b < 0). The specific expressions are shown in Figure 12.

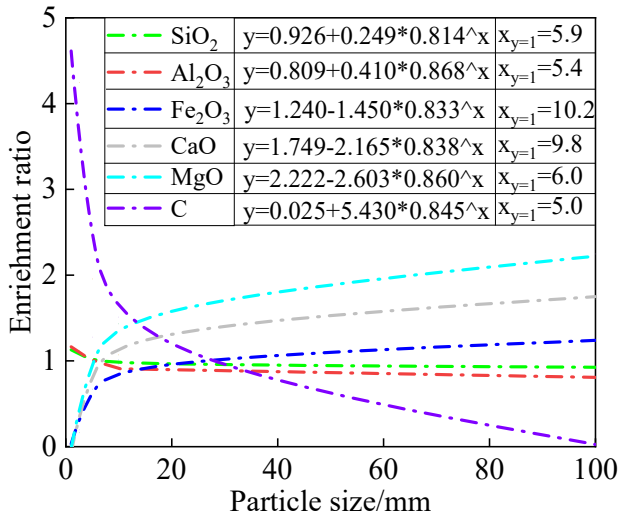

Figure 12. Element enrichment of gangue with different particle sizes.

From the definition of the enrichment ratio, it can be deduced that if θ = y = 1.0, the element enrichment is the same as that of the original gangue. Therefore, according to the expression of the enrichment ratio of each component in gangue at different particle sizes presented in Figure 12, it is clear that the enrichment ratio of SiO_2 is less than that of the original gangue when the particle size is greater than 5.9 mm. The enrichment ratio of Al_2O_3 is smaller than that of the original gangue when the particle size is greater than 5.40 mm. When the particle size exceeds 10.20 mm, the enrichment ratio of C is smaller than that of the original gangue. Similarly, when the particle size is smaller than 9.84, 6.0, and 5.0 mm, the enrichment ratio of Fe_2O_3, CaO, and MgO is correspondingly smaller than in the original gangue. According to the changes of each curve, the enrichment ratios of C, CaO, and MgO change significantly more than those of Fe_2O_3, Al_2O_3, and SiO_2,

which is consistent with the change of the distribution ratio of each component analyzed in Section 3.2.1.

According to a detailed analysis of the variation law of the mineral components of coal gangue with the crushing particle size, the phenomenon of selective crushing occurs in the jaw-crushing process as a result of the different compositions of particles contained in the gangue during the crushing process. As a result, the proportion of particles in the coarse and fine particles is different from the original gangue. Therefore, the materials containing CaO and MgO are broken because they cannot be sufficiently crushed, and the particle size grade tends to be larger. However, particles containing C, SiO_2, Al_2O_3, and other components are vulnerable to impact crushing and enter the fine-grained components.

4. Summary

Through the gangue particle size obtained after jaw crushing and the corresponding composition analysis, the distribution law of particle size and the correlation between the particle size and chemical composition content of the gangue after jaw crushing are obtained, and the following conclusions are drawn:

(1) The R–R formula is used to describe the particle size distribution of gangue crushing at different port widths. The relationship between the characteristic particle size, uniformity index, and port width is obtained through a numerical fitting. Then, the particle size distribution model of gangue after jaw fracture is obtained:

$$R(D_p) = 1 - \exp\left[-\left(\frac{D_p}{7.39 * \ln(\mathrm{x} - 3\ .82)}\right)^{1.399 * x^{(-0.1129)}}\right]$$

(2) By comparing the chemical composition of gangue at different particle size ranges after crushing, it was found that the distribution rate (ε) of SiO_2, Al_2O_3, Fe_2O_3, CaO, and MgO always increased with the increase in the width of the discharge port. The distribution rate (ε) of the C element in the coarse-grained product decreased with the increase of the width of the discharge port. From the $\Delta\varepsilon_{max}$ of each component, it can be concluded that the influence of the width of the discharge port on the distribution rate (ε) of each component is Fe_2O_3 > SiO_2 > Al_2O_3 > C > MgO > CaO.

(3) The gangue exhibits an obvious selective crushing phenomenon in the crushing process. As the width of the discharge port/port increased, the gangue particles containing CaO and MgO were enriched in the coarse-grained products. The enrichment ratio (θ) increased gradually as the discharge port width decreased. The enrichment ratio (θ) of particles containing Fe_2O_3 fluctuated around 1.0 and gradually enriched from fine-grained to coarse-grained with the increased discharge port. The enrichment ratios (θ) of Al_2O_3 and SiO_2 increased slowly with the width of the discharge port, and the range was concentrated between 0.95 and 1.0. The enrichment ratio (θ) of gangue particles containing C was always less than 1.0 and decreased with the increase of the discharge port width.

(4) The variation law of each component of the gangue in the crushed particle size can be obtained, and the distribution rate (ε) of each element showed a law of first rising and then falling. Compared with $\Delta\varepsilon_{max}$, it is evident that the effect of particle size on each component is C>MgO>CaO>Fe_2O_3>Al_2O_3 >SiO_2. The trend of the enrichment ratio (θ) of each component in the broken gangue is consistent with the form $y = a + b * \hat{c}x$. The enrichment ratios of SiO_2, Al_2O_3, and C decreased with the increase in particle size, while MgO, CaO, and Fe_2O_3 decreased with the increase in particle size.

(5) The research results have significance in guiding the selection of resource utilization methods of gangue with different particle sizes after crushing. For example, fine-particle gangue rich in the element C can be used for combustion and power generation; large-particle gangue rich in the elements CaO and MgO can be used for construction materials or road cornerstones, etc. Such selection is helpful to maximize the utilization value of gangue.

Author Contributions: L.Z.: conceptualization, methodology; W.G.: writing—original draft preparation, sample testing, data analysis; T.S.: sample collection and data analysis; F.Q.: data curation. All authors have read and agreed to the published version of the manuscript.

Funding: This research received no external funding.

Institutional Review Board Statement: Not applicable.

Informed Consent Statement: Not applicable.

Data Availability Statement: The original contributions presented in the study are included in the article; further inquiries can be directed to the corresponding author.

Acknowledgments: The authors would like to appreciate the editor and the reviewers for their useful and valuable comments and suggestions.

Conflicts of Interest: The authors declare no conflict of interest.

References

1. Shang, Y.; Yang, F.-L.; Ning, X.; Dong, Y.-R.; Sang, N. Toxicity of Soil Leachate from Coal Gangue and Its Surrounding Village of Barley (Hordeum vulgare). *Huan Jing Ke Xue Huanjing Kexue* **2020**, *41*, 2936–2941. [PubMed]
2. Wang, X.W.; Zhong, N.N.; Hu, D.M.; Liu, Z.Z.; Zhang, Z.H. Polycyclic aromatic hydrocarbon (PAHs) pollutants in groundwater from coal gangue stack area: Characteristics and origin. *Water Sci. Technol.* **2009**, *59*, 1043–1051. [CrossRef] [PubMed]
3. Jiang, X.; Lu, W.X.; Zhao, H.Q.; Yang, Q.C.; Yang, Z.P. Potential ecological risk assessment and prediction of soil heavy-metal pollution around coal gangue dump. *Nat. Hazards Earth Syst. Sci.* **2014**, *14*, 1599–1610. [CrossRef]
4. Zhang, Y.; Ling, T.C. Reactivity activation of waste coal gangue and its impact on the properties of cement-based materials—A review. *Constr. Build. Mater.* **2020**, *234*, 117424. [CrossRef]
5. Haibin, L.; Zhenling, L. Recycling utilization patterns of coal mining waste in China. *Resour. Conserv. Recycl.* **2010**, *54*, 1331–1340. [CrossRef]
6. Zhao, J.; Wang, D.; Liao, S. Effect of mechanical grinding on physical and chemical characteristics of circulating fluidized bed fly ash from coal gangue power plant. *Constr. Build. Mater.* **2015**, *101*, 851–860. [CrossRef]
7. Lü, Q.; Dong, X.; Zhu, Z.; Dong, Y. Environment-oriented low-cost porous mullite ceramic membrane supports fabricated from coal gangue and bauxite. *J. Hazard. Mater.* **2014**, *273*, 136–145. [CrossRef]
8. Dang, W.; He, H.Y. Glass-ceramics fabricated by efficiently utilizing coal gangue. *J. Asian Ceram. Soc.* **2020**, *8*, 365–372. [CrossRef]
9. Xu, G.L.; Sun, C.M.; Sun, Y.; Liao, H. A new comprehensive utilization method for coal gangue: Preparing alite-sulphoaluminate cement. In *Advanced Materials Research*; Trans Tech Publications Ltd.: Bäch, Switzerland, 2013; Volume 652, pp. 1527–1532.
10. Wang, B.; Ma, Y.; Lee, X.; Wu, P.; Liu, F.; Zhang, X.; Li, L.; Chen, M. Environmental-friendly coal gangue-biochar composites reclaiming phosphate from water as a slow-release fertilizer. *Sci. Total Environ.* **2021**, *758*, 143664. [CrossRef]
11. Ashfaq, M.; Heeralal, M.; Moghal, A.A.B. Characterization studies on coal gangue for sustainable geotechnics. *Innov. Infrastruct. Solut.* **2020**, *5*, 1–12. [CrossRef]
12. Lavrinenko, A.A.; Svechnikova, N.Y.; Konovnitsyna, N.S.; Igumensheva, E.A.; Kuklina, O.V.; Khasanzyanova, A.I. Utilization of bituminous coal flotation wastes in the manufacture of ceramic brick. *Solid Fuel Chem.* **2018**, *52*, 406–410. [CrossRef]
13. Wu, C.; Jiang, W.; Zhang, C.; Li, J.; Wu, S.; Wang, X.; Xu, Y.; Wang, W.; Feng, M. Preparation of solid-waste-based pervious concrete for pavement: A two-stage utilization approach of coal gangue. *Constr. Build. Mater.* **2022**, *319*, 125962. [CrossRef]
14. Li, B.; Ju, F. An experimental investigation into the compaction characteristic of granulated gangue backfilling materials modified with binders. *Environ. Earth Sci.* **2018**, *77*, 1–9. [CrossRef]
15. Wu, D.; Luo, F.; Li, M.; Diao, Y.; Guo, Y.; Xu, P. Macroscopic and microscopic study on the compression bearing characteristics and deformation failure mechanism of gangue with different particle sizes. *Powder Technol.* **2021**, *383*, 198–211. [CrossRef]
16. Song, S.; Li, S.; Zhang, T.; Pan, H.; Liu, N.; Zhang, L. Study on the distribution pattern of particle re-crushing in the coal and rock mass crushing process under pressure. *PLoS ONE* **2022**, *17*, e0262235.
17. Li, J.P.; Zheng, K.H.; Du, C.L. The distribution discipline of impact crushed on coal and gangue. *J. China Coal Soc.* **2013**, *38*, 54–58.
18. Yang, D.-L.; Li, J.-P.; Du, C.-L.; Zheng, K.-H.; Liu, S.-Y. Particle size distribution of coal and gangue after impact-crush separation. *J. Cent. South Univ.* **2017**, *24*, 1252–1262. [CrossRef]
19. Zhang, H.; Ouyang, S. Release characteristics of heavy metals from coal gangue under simulation leaching conditions. *Energy Explor. Exploit.* **2014**, *32*, 413–422. [CrossRef]
20. Tang, Q.; Li, L.; Zhang, S.; Zheng, L.; Miao, C. Characterization of heavy metals in coal gangue-reclaimed soils from a coal mining area. *J. Geochem. Explor.* **2018**, *186*, 1–11. [CrossRef]
21. Li, C.; Zheng, L.; Jiang, C.; Chen, X.; Ding, S. Characteristics of leaching of heavy metals from low-sulfur coal gangue under different conditions. *Int. J. Coal Sci. Technol.* **2021**, *8*, 780–789. [CrossRef]
22. Legendre, D.; Zevenhoven, R. Assessing the energy efficiency of a jaw crusher. *Energy* **2014**, *74*, 119–130. [CrossRef]
23. Moghadam, M.J.; Ajalloeian, R.; Hajiannia, A. Preparation and application of alkali-activated materials based on waste glass and coal gangue: A review. *Constr. Build. Mater.* **2019**, *221*, 84–98. [CrossRef]

24. Li, J.; Wang, J. Comprehensive utilization and environmental risks of coal gangue: A review. *J. Clean. Prod.* **2019**, *239*, 117946. [CrossRef]
25. Tan, W.F.; Wang, L.A.; Huang, C. Environmental effects of coal gangue and its utilization. *Energy Sources Part A Recovery Util. Environ. Eff.* **2016**, *38*, 3716–3721. [CrossRef]
26. Yu, L.J.; Feng, Y.L.; Yan, W. The current situation of comprehensive utilization of coal gangue in China. In *Advanced Materials Research*; Trans Tech Publications Ltd.: Bäch, Switzerland, 2012; Volume 524, pp. 915–918.
27. Johansson, M.; Bengtsson, M.; Evertsson, M.; Hulthén, E. A fundamental model of an industrial-scale jaw crusher. *Miner. Eng.* **2017**, *105*, 69–78. [CrossRef]
28. González-Tello, P.; Camacho, F.; Vicaria, J.; González, P. A modified Nukiyama–Tanasawa distribution function and a Rosin–Rammler model for the particle-size-distribution analysis. *Powder Technol.* **2008**, *186*, 278–281. [CrossRef]
29. Allaire, S.E.; Parent, L.E. Size guide number and Rosin–Rammler approaches to describe particle size distribution of granular organic-based fertilisers. *Biosyst. Eng.* **2003**, *86*, 503–509. [CrossRef]
30. Delagrammatikas, G.; Tsimas, S. Grinding process simulation based on Rosin-Rammler equation. *Chem. Eng. Commun.* **2004**, *191*, 1362–1378. [CrossRef]
31. Tambun, R.; Furukawa, K.; Hirayama, M.; Shimadzu, M.; Yamanaka, S.; Ohira, Y. Measurement and Estimation of the Particle Size Distribution by the Buoyancy Weighing–Bar Method and the Rosin–Rammler Equation. *J. Chem. Eng. Jpn.* **2018**, *49*, 229–233. [CrossRef]
32. Sutherland, R.A.; Tolosa, C.A.; Tack, F.M.G.; Verloo, M.G. Characterization of selected element concentrations and enrichment ratiosin background and anthropogenically impacted roadside areas. *Arch. Environ. Contam. Toxicol.* **2000**, *38*, 428–438. [CrossRef]
33. Bourennane, H.; Douay, F.; Sterckeman, T.; Villanneau, E.; Ciesielski, H.; King, D.; Baize, D. Mapping of anthropogenic trace elements inputs in agricultural topsoil from Northern France using enrichment factors. *Geoderma* **2010**, *157*, 165–174. [CrossRef]
34. Reimann, C.; de Caritat, P. Distinguishing between natural and anthropogenic sources for elements in the environment: Regional geochemical surveys versus enrichment factors. *Sci. Total Environ.* **2005**, *337*, 91–107. [CrossRef] [PubMed]
35. Duran, J. *Sands, Powders, and Grains: An Introduction to the Physics of Granular Materials*; Springer Science & Business Media: Berlin/Heidelberg, Germany, 2012.
36. Henningsen, D. Crushing of sedimentary rock samples and its effect on shape and number of heavy minerals. *Sedimentology* **1967**, *8*, 253–255. [CrossRef]
37. Du, F.; Bai, H. Thin Bedrock Coal Seam Overlying Rock Failure Mechanism under the Influence of the Depositional Environment. *Electron. J. Geotech. Eng.* **2012**, *17*, 3373–3384.
38. Kasanin-Grubin, M. Clay mineralogy as a crucial factor in badland hillslope processes. *Catena* **2013**, *106*, 54–67. [CrossRef]
39. Nugroho, S.A.; Wibisono, G.; Ongko, A.; Mauliza, A.Z. The Influence of High Plasticity and Expansive Clay Stabilization with Limestone on Unconfined Compression Strength. *J. Civ. Eng. Forum* **2021**, *7*, 147–154.
40. Cokca, E.; Erol, O.; Armangil, F. Effects of compaction moisture content on the shear strength of an unsaturated clay. *Geotech. Geol. Eng.* **2004**, *22*, 285–297. [CrossRef]